

RESEARCH ARTICLE

Open Access

On a recursive formulation for solving inverse form finding problems in isotropic elastoplasticity

Sandrine Germain^{*}, Philipp Landkammer and Paul Steinmann

^{*}Correspondence:
sandrine.germain@fau.de
University of Erlangen-Nuremberg,
Chair of Applied Mechanics,
Egerlandstrasse 5, 91058 Erlangen,
Germany

Abstract

Background: Inverse form finding methods allow conceiving the design of functional components in less time and at lower costs than with direct experiments. The deformed configuration of the functional component, the applied forces and boundary conditions are given and the undeformed configuration of this component is sought.

Methods: In this paper we present a new recursive formulation for solving inverse form finding problems for isotropic elastoplastic materials, based on an inverse mechanical formulation written in the logarithmic strain space. First, the inverse mechanical formulation is applied to the target deformed configuration of the workpiece with the set of internal variables set to zero. Subsequently a direct mechanical formulation is performed on the resulting undeformed configuration, which will capture the path-dependency in elastoplasticity. The so obtained deformed configuration is furthermore compared with the target deformed configuration of the component. If the difference is negligible, the wanted undeformed configuration of the functional component is obtained. Otherwise the computation of the inverse mechanical formulation is started again with the target deformed configuration and the current state of internal variables obtained at the end of the computed direct formulation. This process is continued until convergence is reached.

Results: In our three numerical examples in isotropic elastoplasticity, the convergence was reached after five, six and nine iterations, respectively, when the set of internal variables is initialised to zero at the beginning of the computation. It was also found that when the initial set of internal variables is initialised to zero at the beginning of the computation the convergence was reached after less iterations and less computational time than with other values. Different starting values for the set of internal variables have no influence on the obtained undeformed configuration, if convergence can be achieved.

Conclusions: With the presented recursive formulation we are able to find an appropriate undeformed configuration for isotropic elastoplastic materials, when only the deformed configuration, the applied forces and boundary conditions are given. An initial homogeneous set of internal variables equal to zero should be considered for such problems.

Keywords: Inverse form finding; Elastoplasticity; Large strain

Background

In this work we present a recursive method for the determination of the undeformed configuration of a functional component, when only the deformed configuration of a workpiece, the applied forces and the boundary conditions are previously known. This is commonly known as an inverse form finding problem, which is inverse to the standard direct kinematic analysis in which the undeformed sheet of metal, the applied forces and boundary conditions are known while the deformed state is sought. Inverse form finding methods are useful because they allow to conceive designs at less time and at lower costs compared to an experimental approach.

Govindjee, 1996 and 1998 [1,2] proposed a numerical method for the determination of the undeformed shape of a continuous body, which is based on the work originally presented in [3]. Their work is limited to isotropic compressible neo-Hookean and incompressible materials. In these contributions it was shown that the weak form of the inverse motion problem based on the Cauchy stress is more efficient and straightforward compared to the weak form based on the Eshelby stress. The governing equation underlying the numerical analysis of the inverse form finding problem is therefore the common weak form of the balance of momentum formulated in terms of the Cauchy stress tensor. The unconventional result lies in the fact that all quantities are parameterised in the spatial coordinates. In [4], temperature changes in the undeformed and deformed configurations have been taken in consideration for orthotropic nonlinear elasticity and axisymmetry using a St.Venant type material, i.e., a material characterised by a quadratic free energy density in terms of the Green-Lagrange strain. Koishi, 2001 [5] used the previous method for the purpose of tire design. Yamada, 1998 [6] proposed another approach as in [1] based on an arbitrary Lagrangian–Eulerian kinematic description. The arbitrary Lagrangian-Eulerian description is approximated by a finite element discretisation. In the last decade, [7,8] extended the method proposed in [1] for the case of anisotropic hyperelasticity for a St.Venant type material. This work is extended in [9,10] to inverse analysis of large-displacement beams in the elastic range. Lu, 2007 [11] proposed a computational method of inverse elastostatics for anisotropic hyperelastic solids in the context of fibrous hyperelastic solids and provide explicit stress function for soft tissue models. In [12] an inverse method for thin-wall structures modelled as geometrically exact stress resultant shells is presented. Germain, 2010 and 2013 [13-15] extended the method originally proposed in [1] to anisotropic hyperelasticity that is based on logarithmic strains. This work was further extended to anisotropic elastoplasticity in [15,16]. The authors demonstrated that the inverse mechanical formulation in elastoplasticity can be used only if the set of internal variables at the deformed state is previously given. However, when dealing with metal forming processes, this set of internal variables is not known at the deformed state. To overcome this problem in anisotropic elastoplasticity, [15,17] proposed a numerical method based on shape optimisation in order to solve inverse form finding problems. A gradient-based shape optimisation is used in the sense of an inverse problem via successive iterations of a direct mechanical problem. The objective function is defined by a least-square minimisation of the difference between the target and the current deformed configuration of the workpiece. The design variables are chosen as the node coordinates stemming from the Finite Element (FE) formulation. A drawback of a node-based shape optimisation is the possible occurrence of mesh distortions. Germain, 2013 and 2012 [15,18,19] proposed a recursive algorithm

using an update of the reference configuration. This proposal allows to avoid mesh distortions but leads to large computational costs. Germain, 2011 and 2012 [20,21] compared the inverse mechanical and the shape optimisation formulation in terms of computational costs and accuracy of the obtained undeformed functional component. They have shown that both methods lead to the same results, but the shape optimisation formulation has larger computational costs. In a similar way [22] dealt with the optimal design and optimal control of structures undergoing large rotations and large elastic deformations. Ibrahimbegovic, 2003 [23] introduced shape optimization of elastic structural systems undergoing large rotations. Sousa, 2002 [24] proposed an approach to optimal shape design in forging. In their recursive formulation the inverse problem is formulated as an optimisation problem, where the objective function sensitivity is calculated by the accumulated sensitivities of the nodal coordinates throughout the entire simulation of the process. Ponthot, 2006 [25] presented optimisation methodologies for automatic parameter identification and shape/process optimisation in metal forming simulation. In the sensitivity analysis they used a disturbed balanced configuration, which is updated until the residual equilibrium of the disturbed problem ends under a fixed tolerance. Recently, [26] proposed an inverse-motion-based form finding for electroelasticity to improve the design and accuracy in electroelastic applications such as grippers, sensors and seals.

In order to overcome the large computational costs ([20,21]) in shape optimisation and the fact that the set of internal variables is unknown at the deformed state, we propose, in this contribution, a new method for solving inverse form finding problems in isotropic elastoplasticity based on the inverse mechanical formulation originally proposed in [1].

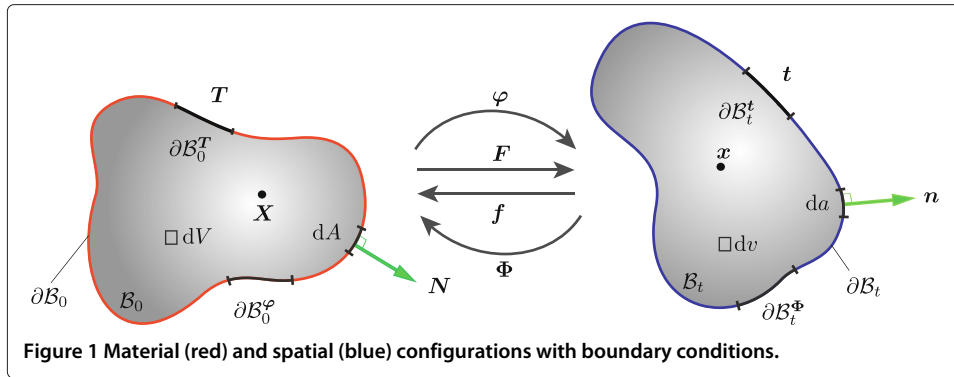
The present work is organised as follows: In order to introduce the utilised notations, the kinematics of geometrically nonlinear continuum mechanics are presented at first. Furthermore a macroscopical phenomenological isotropic elastoplastic model based on the additive decomposition of the total strains in the logarithmic strain space is introduced. A direct and an inverse mechanical formulations for determining the deformed and the undeformed configurations of a workpiece are respectively presented. A recursive formulation for solving the inverse form finding problem in isotropic elastoplasticity is developed using both previously presented formulations. To illustrate the proposed recursive formulation three numerical examples are presented. The influence of the starting values for the set of internal variables at the beginning of the computation is finally discussed.

Methods

Kinematics of geometrically nonlinear continuum mechanics

In this section we introduce the notations, similar to [13], by briefly recalling the basic kinematic quantities of geometrically nonlinear continuum mechanics. Let \mathcal{B}_0 denote the material configuration or undeformed shape of a continuum body parameterised by material coordinates X at time $t = 0$ and \mathcal{B}_t the corresponding spatial configuration or deformed shape parameterised by spatial coordinates x at time t , as depicted in Figure 1. The boundary of \mathcal{B}_0 and \mathcal{B}_t is assumed to be decomposed into disjoint parts, so that

$$\partial\mathcal{B}_0 = \partial\mathcal{B}_0^{\bar{T}} \cup \partial\mathcal{B}_0^{\bar{\varphi}} \quad \text{with} \quad \partial\mathcal{B}_0^{\bar{T}} \cap \partial\mathcal{B}_0^{\bar{\varphi}} = \emptyset \quad (1)$$



and

$$\partial B_t = \partial B_t^{\bar{t}} \cup \partial B_t^{\bar{\Phi}} \quad \text{with} \quad \partial B_t^{\bar{t}} \cap \partial B_t^{\bar{\Phi}} = \emptyset, \quad (2)$$

where $\partial B_0^{\bar{t}}$ and $\partial B_t^{\bar{t}}$ are the Neumann type boundary conditions and $\partial B_0^{\bar{\Phi}}$ and $\partial B_t^{\bar{\Phi}}$ are the Dirichlet type boundary conditions. In the usual direct mechanical formulation, the material configuration is given and the objective is to determine the direct deformation map φ as

$$\mathbf{x} = \varphi(\mathbf{X}) : B_0 \longrightarrow B_t. \quad (3)$$

The corresponding direct deformation gradient together with its Jacobian determinant are defined as

$$\mathbf{F} = \nabla_{\mathbf{X}} \varphi, \quad J = \det \mathbf{F} > 0. \quad (4)$$

$\nabla_{\mathbf{X}}$ denotes the gradient operator with respect to the material coordinates \mathbf{X} . On the contrary, in the inverse mechanical formulation, the spatial configuration is given and the inverse deformation map Φ has to be determined as

$$\mathbf{X} = \Phi(\mathbf{x}) : B_t \longrightarrow B_0. \quad (5)$$

The corresponding inverse deformation gradient together with its Jacobian determinant are given by

$$\mathbf{f} = \nabla_{\mathbf{x}} \Phi, \quad j = \det \mathbf{f} > 0. \quad (6)$$

Again, $\nabla_{\mathbf{x}}$ denotes the gradient operator with respect to the spatial coordinates \mathbf{x} . It follows immediately from the above definitions, that the inverse deformation map denotes a nonlinear map inverse to the deformation map of the direct problem

$$\Phi = \varphi^{-1}. \quad (7)$$

Thus, the inverse and direct deformation gradients together with their Jacobian determinants are simply related through an algebraic inversion

$$\mathbf{f} = \mathbf{F}^{-1} \quad \text{and} \quad j = J^{-1}. \quad (8)$$

Nonlinear isotropic elastoplastic material model in the logarithmic strain space

Several discussions occurred in the last decades in the mechanical community on the use or not of the additive decomposition of the total strain proposed by [27] for large strains

as in the small strain theory in comparison with the use of the multiplicative decomposition of the deformation gradient proposed by [28], see for example [29] or [30]. In his book Ibrahimbegovic [31] wrote on page 338 “abandon any formulation of large strain plasticity using an additive decomposition of the the total strain”. For these reasons when dealing with elastoplasticity at large strains the multiplicative decomposition of the deformation gradient is widely used, see for example [31-33] or [34]. Nevertheless [35] and [36] proposed in their papers an alternative formulation for elastoplasticity at large strains which is a modular macroscopic phenomenological approach formulated in Lagrangian logarithmic strain. They also showed that in metal plasticity (small elastic but large plastic deformations), as in our case, the obtained results with the multiplicative formulation and the additive decomposition in the logarithmic strain space are close to each other. Apel, 2004 [36] and [37] compared as well the performances of the two approaches for sheet drawing processes and concluded that for the range of metal plasticity at moderate elastic strains the results are closed to each other, while the additive formulation provides simpler and more efficient settings. In the subsequent, we present the material model in the logarithmic strain space as proposed in [35] and [36], that we used for a matter of convenience and for a better utilisation of our recursive formulation for solving inverse form finding problems. Three steps are required for the use of the modular approach in large strain: a “geometric preprocessor”, the constitutive model and a “geometric postprocessor”. In the logarithmic strain space, the total strain is first written as a function of the right Cauchy–Green tensor \mathbf{C}

$$\mathbf{E} = \frac{1}{2} \ln(\mathbf{C}) = \frac{1}{2} \ln(\mathbf{F}^T \cdot \mathbf{F}) = \frac{1}{2} \sum_{i=1}^3 \ln(\lambda_i) \mathbf{M}_i, \quad (9)$$

where $\lambda_{i=1,2,3}$ are the eigenvalues of \mathbf{C} , i.e. squares of the principal stretches and $\mathbf{M}_{i=1,2,3}$ the associated eigenvalue bases (see for example [38]). The total strains are then decomposed into an elastic and a plastic part using an additive Lagrangian formulation

$$\mathbf{E} = \mathbf{E}^e + \mathbf{E}^p. \quad (10)$$

It can be seen that the structure adopted from the geometrically linear theory is conserved. The first and second derivatives of the logarithmic strain with respect to the right Cauchy–Green strain [38] are defined by

$$\mathbb{P} = 2 \frac{\partial \mathbf{E}}{\partial \mathbf{C}} \quad \text{and} \quad \mathbb{L} = 2 \frac{\partial \mathbb{P}}{\partial \mathbf{C}}. \quad (11)$$

In a second step the total and logarithmic strains enter in the additive format a constitutive model, that defines the stresses and consistent tangents work-conjugate to the logarithmic strain measure. Considering the first and second law of thermodynamics, the reduced Clausius–Duhem inequality is written as

$$\mathcal{D} = \mathbf{T} : \dot{\mathbf{E}} - \dot{\psi} \geq 0, \quad (12)$$

where $(\dot{\cdot})$ denotes the material time derivative. The total free energy density ψ is decomposed into an elastic and a plastic part

$$\begin{aligned} \psi(\mathbf{E}, \mathbf{E}^p, \alpha) &= \psi^e(\mathbf{E} - \mathbf{E}^p) + \psi^p(\alpha) \\ \Rightarrow \psi(\mathbf{E}^e, \alpha) &= \psi^e(\mathbf{E}^e) + \psi^p(\alpha), \end{aligned} \quad (13)$$

where (\mathbf{E}^p, α) is the set of internal variables, α denotes a scalar variable that models isotropic hardening. The elastic part of the free energy density depends only on the elastic part of the total strains and on the material parameters λ and μ

$$\psi^e(\mathbf{E}^e) = \frac{1}{2}\lambda \operatorname{tr}(\mathbf{E}^e)^2 + \mu \operatorname{tr}((\mathbf{E}^e)^2). \quad (14)$$

λ and μ are the Lamé parameters and $\operatorname{tr}(\cdot)$ is the trace of the corresponding tensor. The plastic part of the free energy density which models nonlinear isotropic hardening reads

$$\psi^p(\alpha) = \frac{1}{2}h\alpha^2 + [\sigma_\infty - \sigma_0] \left[\alpha + \frac{e^{-w\alpha}}{w} \right], \quad (15)$$

where h , σ_0 , σ_∞ and w are also material parameters, i.e., the isotropic hardening parameter, the initial yield stress, the infinite yield stress and the saturation parameter, which defines the nonlinearity of the hardening, respectively. \mathbf{T} in Equation 12 is defined as the Lagrangian stress tensor work-conjugate to the logarithmic strain measure \mathbf{E}

$$\mathbf{T} = \frac{\partial \psi^e}{\partial \mathbf{E}^e} = \lambda \operatorname{tr}(\mathbf{E}^e) \mathbf{I} + 2\mu \mathbf{E}^e. \quad (16)$$

With the definition of the free energy density in Equation 13, the Clausius-Duhem inequality can be reduced to

$$\mathcal{D} = \mathbf{T} : \dot{\mathbf{E}}^p - \frac{\partial \psi}{\partial \alpha} \dot{\alpha} \geq 0. \quad (17)$$

The yield surface is defined by

$$\mathcal{Y} = \{ \mathbf{T} \mid \Phi(\mathbf{T}, \frac{\partial \psi}{\partial \alpha}) - \sqrt{\frac{2}{3}}\sigma_0 = 0 \}, \quad (18)$$

where Φ is the yield function defined as

$$\Phi(\mathbf{T}, \frac{\partial \psi}{\partial \alpha}) = \|\operatorname{dev}(\mathbf{T})\| - \sqrt{\frac{2}{3}} \frac{\partial \psi}{\partial \alpha}. \quad (19)$$

The evolution laws for the internal variables, with an associative plasticity model, are determined with the principle of maximum plastic dissipation. The following plastic flow rule and hardening law are characterised by

$$\dot{\mathbf{E}}^p = \dot{\gamma} \frac{\operatorname{dev}(\mathbf{T})}{\|\operatorname{dev}(\mathbf{T})\|} \quad (20)$$

and

$$\dot{\alpha} = \dot{\gamma} \sqrt{\frac{2}{3}}, \quad (21)$$

where $\dot{\gamma}$ is the plastic multiplier determined by the Kuhn–Tucker-type loading-unloading conditions and $\operatorname{dev}(\mathbf{T})$ denotes the deviatoric part of the tensor \mathbf{T} . In the subsequent numerical examples, the isotropic elastoplastic constitutive initial value problem is solved by a return mapping algorithm (or plastic corrector step) following the one presented in [33] for J2 plasticity. In a third step the components of the logarithmic space are mapped back to the nominal stresses and moduli by a "geometric postprocessor". The second Piola–Kirchhoff stress \mathbf{S} is then expressed by

$$\mathbf{S} = \mathbf{T} : \mathbb{P}. \quad (22)$$

The associated elastoplastic modulus \mathbb{C}^{ep} that is defined by setting the rate of the Piola–Kirchhoff tensor as a function of the Lagrangian rate $\dot{\mathbf{C}}/2$ is given by

$$\mathbb{C}^{ep} = \mathbb{P}^T : \mathbb{E}^{ep} : \mathbb{P} + \mathbf{T} : \mathbb{L}. \quad (23)$$

The transposition symbol refers to an exchange of the first and last pairs of index. \mathbb{E}^{ep} is the fourth-order elastoplastic tangent modulus (see for example [32]).

Direct mechanical problem for determining the deformed shape from equilibrium

Before introducing the inverse boundary value problem in the subsequent section we present briefly the direct mechanical problem, where the undeformed configuration of the workpiece, the applied forces and boundary conditions are given, whereas the deformed configuration of the workpiece is sought. As in [13,15] the direct mechanical problem for determining the deformed shape from equilibrium is defined by

$$\begin{aligned} \text{Div}(\mathbf{P}) &= \mathbf{0} && \text{in } \mathcal{B}_0, \\ \mathbf{P} \cdot \mathbf{N} &= \bar{\mathbf{T}} && \text{on } \partial\mathcal{B}_0^{\bar{\mathbf{T}}}, \\ \boldsymbol{\varphi} &= \bar{\boldsymbol{\varphi}} && \text{on } \partial\mathcal{B}_0^{\bar{\boldsymbol{\varphi}}}, \end{aligned} \quad (24)$$

where $\bar{\mathbf{T}}$ is a given traction per unit area in the material configuration (Neumann boundary condition) and $\bar{\boldsymbol{\varphi}}$ is a given boundary deformation (Dirichlet boundary condition), which are illustrated in Figure 1. \mathbf{P} is the Piola stress tensor. The weak form of the direct boundary value problem reads

$$\mathbf{G}(\boldsymbol{\varphi}, \boldsymbol{\eta}; \mathbf{X}) = \int_{\partial\mathcal{B}_0^{\bar{\mathbf{T}}}} \boldsymbol{\eta} \cdot \bar{\mathbf{T}} dA - \int_{\mathcal{B}_0} \text{Grad } \boldsymbol{\eta} : \mathbf{P} dV = 0, \quad (25)$$

where $\boldsymbol{\eta}$ is an arbitrary weighting function with the property $\boldsymbol{\eta} \in \mathcal{V} = \{\boldsymbol{\eta} \mid \boldsymbol{\eta} = \mathbf{0} \text{ on } \partial\mathcal{B}_0^{\bar{\boldsymbol{\varphi}}}\}$. The determination of the deformed configuration \mathcal{B}_t is performed by the Finite Element Method (FEM). \mathcal{B}_0 is discretised into n_{el} elements. The weak form of the direct boundary value problem becomes thereby a nonlinear system of equations, which is solved by the Newton–Raphson method. A linearisation of the weak form is thus performed and gives the needed tangent stiffness matrix of the direct problem. Here we recall the tangent stiffness matrix for the direct mechanical formulation

$$\mathbf{k}^{(ij)} := \mathbf{A} \int_{\mathcal{B}_0^e} \nabla_X N^{(i)} \cdot \frac{\partial \mathbf{P}}{\partial \mathbf{F}} \cdot \nabla_X N^{(j)} dV \quad (26)$$

with

$$\frac{\partial \mathbf{P}}{\partial \mathbf{F}} = [\mathbf{F} \bar{\otimes} \mathbf{I}] : \mathbb{C}^{ep} : [\mathbf{F}^t \bar{\otimes} \mathbf{I}] + \mathbf{I} \bar{\otimes} \mathbf{S}, \quad (27)$$

where (i, j) are the node numbers, \cdot denotes the contraction with the second index of the corresponding tangent operator and $\bar{\otimes}$ denotes a non-standard dyadic product with $[\mathbf{A} \bar{\otimes} \mathbf{B}]_{ijkl} = A_{ik} B_{jl}$. Due to the computation of the direct mechanical formulation the path-dependency, which has to be considered in elastoplasticity, is ensured.

Inverse mechanical problem for determining the undeformed shape from equilibrium

The inverse form finding problem consists in the determination of the undeformed configuration of a functional component, when only the deformed configuration of a workpiece, the applied forces and the boundary conditions are previously known. Written as an optimisation problem (for more details see the subsequent “Form finding optimisation scheme” Section) the goal is to find the undeformed configuration of a workpiece by minimising the difference between the target deformed configuration and the computed deformed configuration with the direct mechanical problem as presented above. The undeformed configuration of the workpiece represents the vector of variables.

The minimisation problem is also subjected to constraints which fulfill the kinematics, the stresses, the boundary value problem, the Karush–Kuhn–Tucker conditions, the consistency condition and the evolution law. The inverse form finding problem can also be formulated from the equilibrium by defining the subsequent inverse boundary value problem, as in [13,15],

$$\begin{aligned} \operatorname{div}(\boldsymbol{\sigma}) &= \mathbf{0} && \text{in } \mathcal{B}_t, \\ \boldsymbol{\sigma} \cdot \mathbf{n} &= \bar{\mathbf{t}} && \text{on } \partial\mathcal{B}_t^{\bar{\mathbf{t}}}, \\ \boldsymbol{\Phi} &= \bar{\boldsymbol{\Phi}} && \text{on } \partial\mathcal{B}_t^{\bar{\boldsymbol{\Phi}}}, \end{aligned} \quad (28)$$

where $\bar{\mathbf{t}}$ is a given traction per unit area in the spatial configuration (Neumann boundary condition) and $\bar{\boldsymbol{\Phi}}$ is a given boundary deformation (Dirichlet boundary condition), which are illustrated in Figure 1. The symmetric Cauchy stress $\boldsymbol{\sigma}$ in the inverse boundary value problem is obtained from the Piola–Kirchhoff stress \mathbf{S} by a push-forward according to

$$\boldsymbol{\sigma} = j\mathbf{F} \cdot \mathbf{S} \cdot \mathbf{F}^T. \quad (29)$$

The weak form of the inverse boundary value problem reads

$$\mathbf{g}(\boldsymbol{\Phi}, \boldsymbol{\eta}; \mathbf{x}) = \int_{\partial\mathcal{B}_t^{\bar{\mathbf{t}}}} \boldsymbol{\eta} \cdot \bar{\mathbf{t}} da - \int_{\mathcal{B}_t} \operatorname{grad} \boldsymbol{\eta} : \boldsymbol{\sigma} dv = 0, \quad (30)$$

where $\boldsymbol{\eta}$ is an arbitrary weighting function with the property $\boldsymbol{\eta} \in \mathcal{V} = \{\boldsymbol{\eta} \mid \boldsymbol{\eta} = \mathbf{0} \text{ on } \partial\mathcal{B}_t^{\bar{\boldsymbol{\Phi}}}\}$. The particular feature of this formulation is that all integrals extend over the spatial configuration, which is given, and all quantities are parameterised in the given spatial coordinates \mathbf{x} . The determination of the undeformed configuration \mathcal{B}_0 is performed by the Finite Element Method (FEM) as for the direct boundary value problem. \mathcal{B}_t is discretised into n_{el} elements as \mathcal{B}_0 . The weak form of the inverse boundary value problem becomes also a nonlinear system of equations, which is also solved by the Newton–Raphson method. A linearisation of the weak form is thus performed and gives the needed tangent stiffness matrix of the inverse problem

$$\mathbf{K}^{(ij)} := \sum_{e=1}^{n_{el}} \int_{\mathcal{B}_t^e} \nabla_{\mathbf{x}} N^{(i)} \cdot \frac{\partial \boldsymbol{\sigma}}{\partial \mathbf{f}} \cdot \nabla_{\mathbf{x}} N^{(j)} dv, \quad (31)$$

with

$$\frac{\partial \boldsymbol{\sigma}}{\partial \mathbf{f}} = \boldsymbol{\sigma} \otimes \mathbf{F}^t - \mathbf{F} \otimes \boldsymbol{\sigma} + j\mathbf{F} \cdot \left[\frac{1}{2} \mathbb{C}^{ep} : \frac{\partial \mathbf{C}}{\partial \mathbf{f}} \right] \cdot \mathbf{F}^t - \boldsymbol{\sigma} \otimes \mathbf{F} \quad (32)$$

where (i, j) are the node numbers, \cdot denotes the contraction with the second index of the corresponding tangent operator and \otimes denotes a non-standard dyadic product with $[\mathbf{A} \otimes \mathbf{B}]_{ijkl} = A_{il}B_{jk}$. For more details see [13] or [15]. Furthermore [15,16] demonstrated that this inverse mechanical formulation might be used in elastoplasticity, when the set of internal variables at the deformed state is given and remains constant during the iterations. Since however in sheet metal forming processes the set of internal variables is not known at the deformed state, this formulation can not be used because the undeformed configuration will thus not be unique.

Form finding optimisation scheme

- Find \mathbf{X} such that

$$f(\mathbf{X}) = \frac{1}{2} \|\boldsymbol{\varphi}(\mathbf{X}) - \mathbf{x}^{\text{target}}\|^2 \rightarrow \min_{\mathbf{X}}$$

- Subject to:
 1. $\mathbf{F} = \nabla_X \boldsymbol{\varphi}, \mathbf{C} = \mathbf{F}^T \cdot \mathbf{F}, \mathbf{E} = \frac{1}{2} \ln \mathbf{C}, \mathbf{E} = \mathbf{E}^e + \mathbf{E}^p$
 2. $\mathbf{T} = \mathbb{E} : \mathbf{E}^e, \mathbf{S} = \mathbf{T} : \mathbb{P}, \mathbf{P} = \dot{\mathbf{F}} \cdot \mathbf{S}$
 3. $\text{Div}(\mathbf{P}) = \mathbf{0}, \mathbf{P} \cdot \mathbf{N} = \overline{\mathbf{T}}, \boldsymbol{\varphi} = \overline{\boldsymbol{\varphi}}$
- and along trajectory $\mathbf{x} = \mathbf{x}(t)$ with $\mathbf{x}(0) = \mathbf{X}, \forall t$:
 1. $\Phi \leq 0, \dot{\gamma} \geq 0, \dot{\gamma} \Phi = 0$ with $\Phi = \Phi(\mathbf{T}, \alpha)$ and $\dot{\alpha} = \dot{\gamma} \sqrt{\frac{2}{3}}$
 2. $\dot{\gamma} \dot{\Phi} = 0$
 3. $\dot{\mathbf{E}}^p = \dot{\gamma} \frac{\partial \Phi}{\partial \mathbf{T}}$

Recursive formulation for solving inverse form finding problems

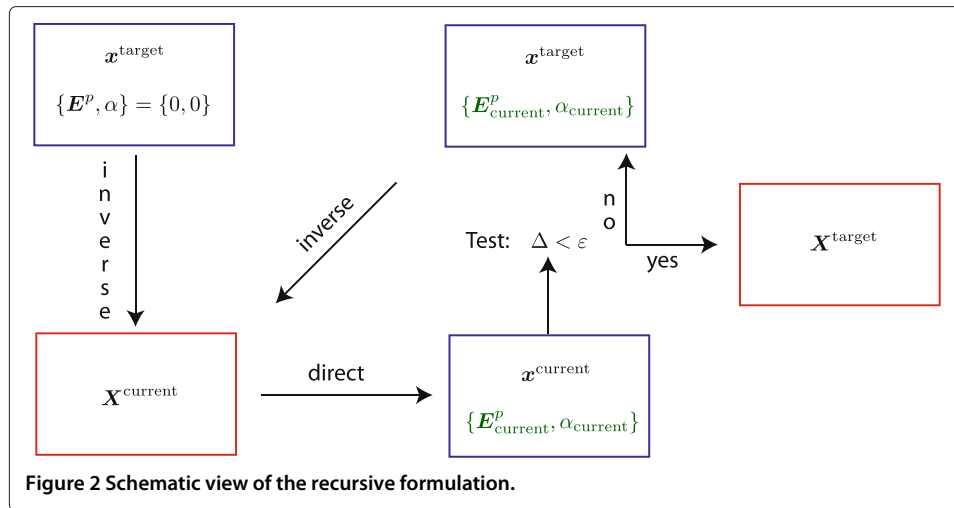
In order to avoid this problem, we developed a recursive algorithm in which we used both direct and inverse mechanical formulations. At the beginning, the set of internal variables is initialised to a homogeneous field equal to zero, i.e., $(\mathbf{E}^p, \alpha) = (0, 0)$. The inverse mechanical formulation in elastoplasticity, as presented above, is performed with the target deformed configuration of the functional component $\mathbf{x}^{\text{target}}$ as well as the applied forces and boundary conditions. The total force is applied in one load step [16]. Thus, an undeformed configuration $\mathbf{X}^{\text{current}}$ is obtained. This undeformed configuration is then used as starting value in the direct mechanical formulation, as presented above. Total force is decomposed into several load steps in order to capture the path-dependency. The obtained internal variables are used as starting value in the next iteration and so on and so forth. Since the direct mechanical formulation in elastoplasticity gives an unique deformed configuration $\mathbf{x}^{\text{current}}$ the corresponding heterogeneous set of internal variables $(\mathbf{E}_{\text{current}}^p, \alpha_{\text{current}})$ is thus unique. The obtained deformed configuration $\mathbf{x}^{\text{current}}$ is then compared with the target deformed configuration $\mathbf{x}^{\text{target}}$ by calculating

$$\Delta = \|\mathbf{x}^{\text{target}} - \mathbf{x}^{\text{current}}(\mathbf{X}^{\text{current}})\|^2. \quad (33)$$

If $\Delta < \varepsilon$ is verified with $\varepsilon = 10^{-8}$, for example, the target undeformed configuration of the functional component $\mathbf{X}^{\text{target}}$ is obtained. If the convergence tolerance yet is not reached, the target deformed configuration $\mathbf{x}^{\text{target}}$, the applied forces, the boundary conditions and now also the heterogeneous field of the internal variables, obtained from the direct mechanical problem, i.e., $(\mathbf{E}^p, \alpha) = (\mathbf{E}_{\text{current}}^p, \alpha_{\text{current}})$, are used as starting values in the next elastoplastic inverse mechanical formulation. This recursive procedure is continued until convergence is reached. Figure 2 resumes schematically the recursive formulation. Note that Equation 33 does not differ from the objective function used in [15,17] for solving inverse form finding problems based on shape optimisation.

Remark:

- If the set of internal variables is again set to a homogeneous field equal to zero and not updated to the heterogeneous field $(\mathbf{E}_{\text{current}}^p, \alpha_{\text{current}})$ in the inverse computation the wanted undeformed configuration will not be reached.



Experiments and results

In this section, the previously presented method for solving inverse form finding problems in isotropic elastoplasticity is evaluated by three numerical examples. Since elastoplasticity is a path-dependent problem, the applied forces in the direct computation are decomposed in several load steps. After each load step the heterogeneous set of internal variables obtained at the equilibrium is used for the initialisation of the Newton–Raphson method in order to reach the equilibrium at the next load step. The inverse computation is performed with only one load step because the plastic strains are given and frozen, so that the problem remains elastic (Equation 10). The obtained final undeformed configurations are plotted. The undeformed configurations are subsequently taken as an input for the direct mechanical formulation. The evolution of the obtained deformed configuration after the last iteration, on which the equivalent plastic strain is plotted, is shown. The equivalent plastic strain is obtained according to:

$$E_{eq}^p = \sqrt{\frac{2}{3} [(E_{11}^p)^2 + (E_{22}^p)^2 + (E_{33}^p)^2 + 2(E_{12}^p)^2 + 2(E_{23}^p)^2 + 2(E_{31}^p)^2]}. \quad (34)$$

The internal variables are initialised to zero at the beginning of the computation. The convergence tolerance was set to $\varepsilon = 10^{-8}$. Each numerical example was computed on an Intel Core2 Duo (2533 MHz).

Numerical example 1: bar

The first example deals with a benchmark problem consisting of the traction of a bar. When using the newly presented method for solving inverse form finding problems in elastoplasticity, the straight form of the bar is considered as the deformed configuration. The deformed configuration of the bar is illustrated in Figure 3. The forces are applied on the top of the bar in vertical direction (red arrows). The bottom of the bar is fixed in the three directions (blue squares). The bar has a 10 mm square base and is 20 mm high. The discretisation is obtained with MSC.Patran2010.2, where hexahedral elements are used. The number of nodes is equal to 45 and the number of elements is 16. The applied force is set to 45000 units of force and decomposed in 20 load steps in the direct computation. The isotropic elastoplastic material parameters used in the simulation are summarised in

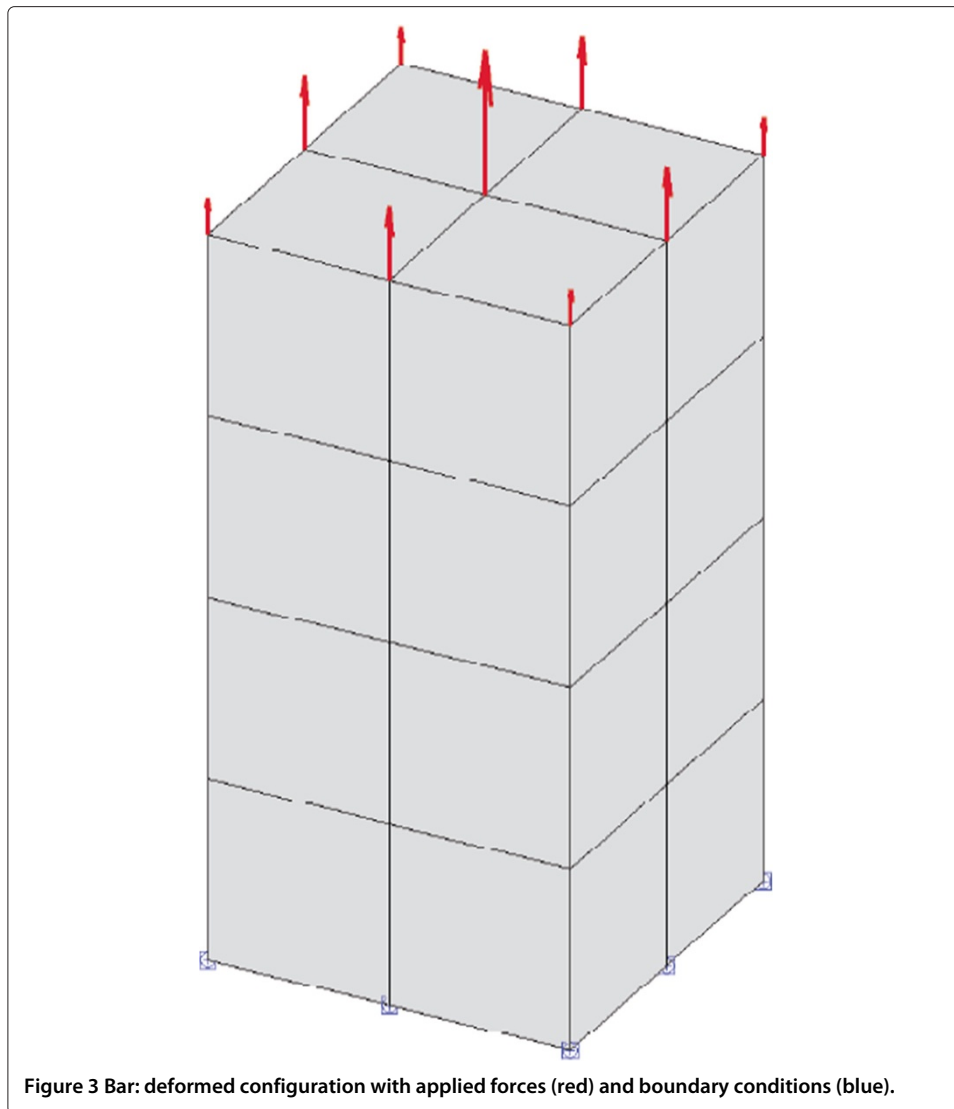


Table 1. The computation of the recursive method took 6 minutes 3 seconds. Six iterations were needed to reach ε . The Δ values introduced in Equation 33 computed after each iteration are shown in Table 2 and plotted on Figure 4 (blue curve). It can be observed that the rate of convergence is almost linear. The finally obtained undeformed configuration of the bar (after iteration six) is illustrated in Figure 5(A) with loads and boundary conditions. The direct mechanical computation with this undeformed configuration as an input is shown in Figure 5(B) with the equivalent plastic strain (-).

Table 1 Material parameters

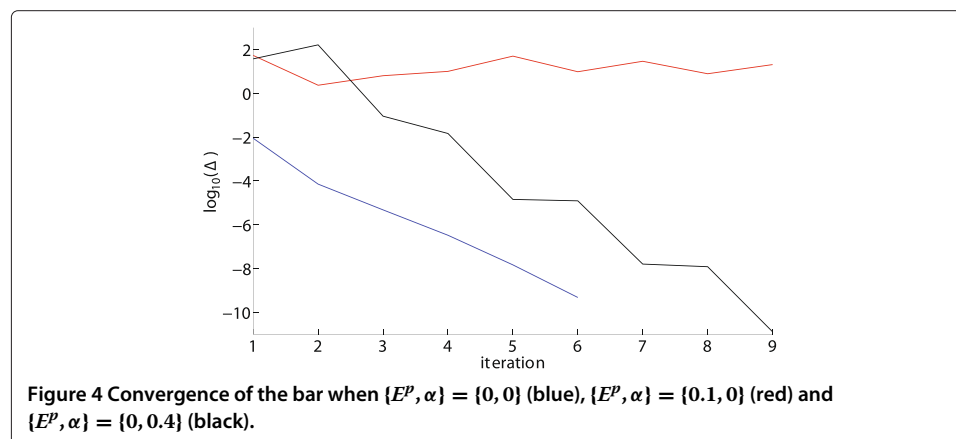
Material parameters	
E	211000 MPa
ν	0.3
h	100 MPa
σ_0	415 MPa
σ_∞	750 MPa
w	15

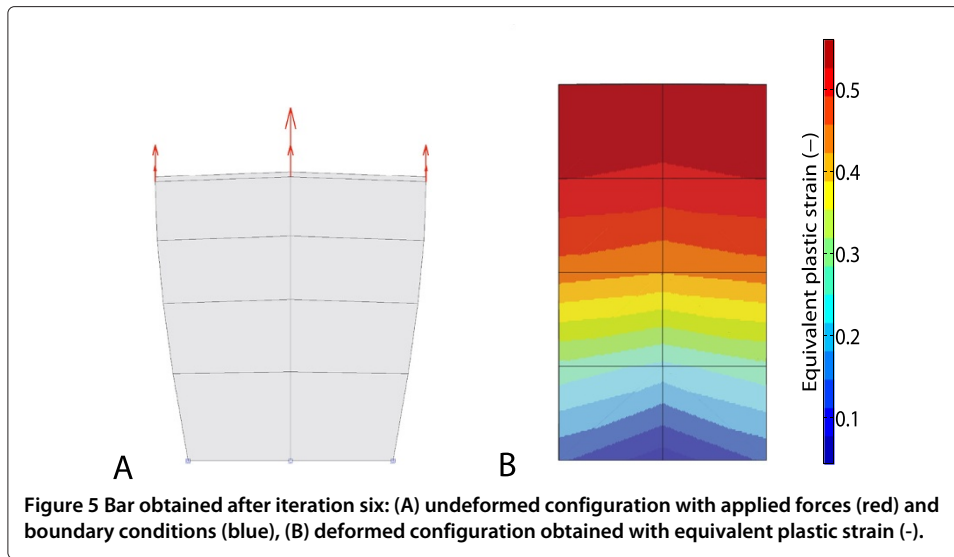
Table 2 Bar: Convergence

Bar: Calculation of Δ			
Iteration	$\{E^p, \alpha\} = \{0, 0\}$	$\{E^p, \alpha\} = \{0.1, 0\}$	$\{E^p, \alpha\} = \{0, 0.4\}$
1	$8.8532 \cdot 10^{-3}$	53.7853	37.5161
2	$7.1592 \cdot 10^{-5}$	2.3427	163.3108
3	$4.7781 \cdot 10^{-6}$	6.3799	$9.0531 \cdot 10^{-2}$
4	$3.303 \cdot 10^{-7}$	10.0643	$1.4682 \cdot 10^{-2}$
5	$1.4706 \cdot 10^{-8}$	49.9705	$1.4356 \cdot 10^{-5}$
6	$4.7759 \cdot 10^{-10}$	9.6875	$1.2357 \cdot 10^{-5}$
7		29.0923	$1.6002 \cdot 10^{-8}$
8		7.8441	$1.2104 \cdot 10^{-8}$
9		20.5272	$1.2903 \cdot 10^{-11}$

Numerical example 2: Cook’s membrane

The second example deals with the Cook’s membrane in 3D. When using the newly presented method for solving inverse form finding problems in elastoplasticity, the straight form of the Cook’s membrane is considered as the deformed configuration. The deformed configuration of the membrane is illustrated in Figure 6. The forces are applied on the right hand side acting from the bottom to the top (red arrows). The left hand side of the membrane is fixed in the three directions (blue squares). The dimensions of the membrane are the same as in [19]. The membrane is discretised by hexahedral elements with MSC.Patran2010.2. The number of nodes is equal to 780 and the number of elements is 528. The applied force is set to 1000 units of force and decomposed in 20 load steps in the direct computation. The isotropic elastoplastic material parameters used in the simulation are summarised in Table 1. The computation of the recursive method took 5 hours 58 minutes 53 seconds. Nine iterations were needed to reach ε . The Δ values introduced in Equation 33 computed after each iteration are summarised in Table 3 and plotted on Figure 7 (blue curve). It can be observed that the rate of convergence is almost linear. Compared to the algorithm presented in [19] for solving inverse form finding problems in elastoplasticity the recursive formulation proposed in this contribution is more efficient regarding the computational costs. The finally obtained undeformed configuration of the Cook’s membrane (after iteration nine) is illustrated in Figure 8(A) with loads and boundary conditions. The direct mechanical computation with this undeformed configuration as an input is shown in Figure 8(B) with the equivalent plastic strain (-).





Numerical example 3: circular, flat plate

The third example deals with a circular, flat plate in 3D. When using the newly presented method for solving inverse form finding problems in elastoplasticity, the circular, flat form of the plate is considered as the deformed configuration. The deformed configuration of the circular, flat plate is illustrated in Figure 9. The applied forces are plotted in red. The inner hole is fixed in three directions (blue squares). The outer hole is set to 95 mm, whereas the inner hole is equal to 75 mm. The circular, flat plate has a thickness of 3 mm.

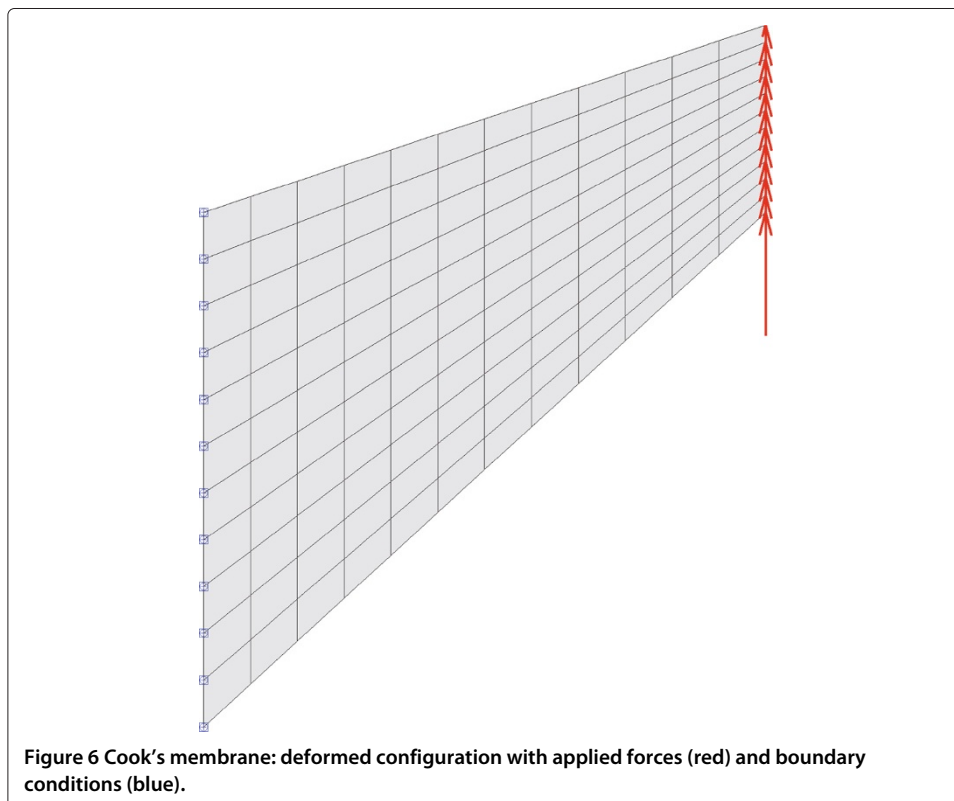


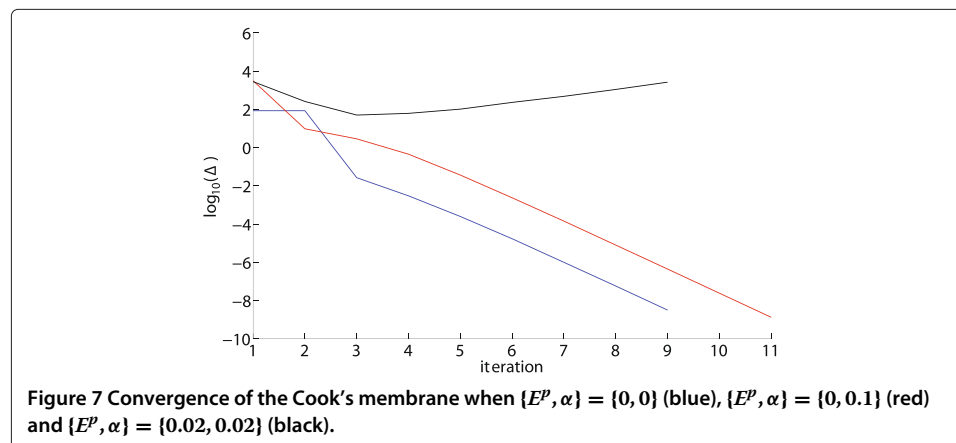
Table 3 Cook's membrane: Convergence

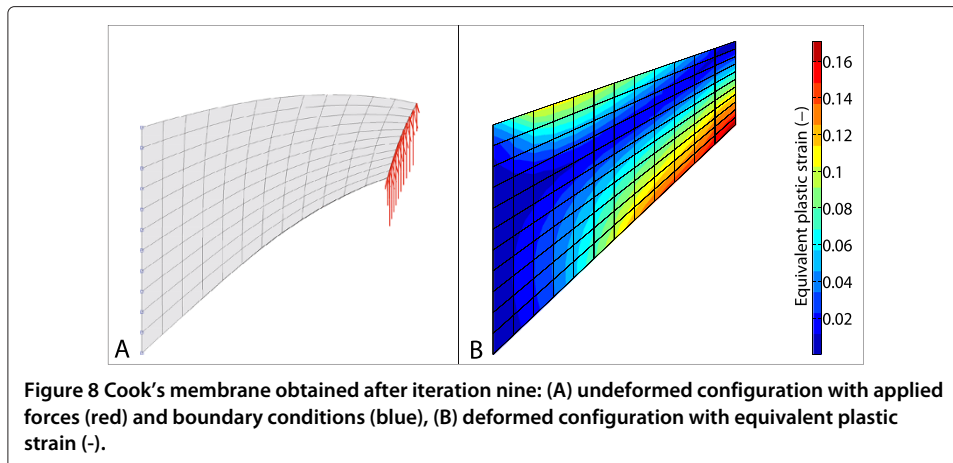
Cook's membrane: Calculation of Δ			
Iteration	$\{E^p, \alpha\} = \{0, 0\}$	$\{E^p, \alpha\} = \{0, 0.1\}$	$\{E^p, \alpha\} = \{0.02, 0.02\}$
1	84.5661	3124.0123	2811.6881
2	$5.8472 \cdot 10^{-2}$	9.5801	257.2319
3	$2.6557 \cdot 10^{-2}$	2.8556	49.982
4	$2.9812 \cdot 10^{-3}$	$4.5033 \cdot 10^{-1}$	61.4643
5	$2.4846 \cdot 10^{-4}$	$3.6374 \cdot 10^{-2}$	102.2576
6	$1.6952 \cdot 10^{-5}$	$2.3578 \cdot 10^{-3}$	229.8063
7	$9.859 \cdot 10^{-7}$	$1.4145 \cdot 10^{-4}$	477.2713
8	$5.7253 \cdot 10^{-8}$	$7.924 \cdot 10^{-6}$	1092.9303
9	$3.1401 \cdot 10^{-9}$	$4.4152 \cdot 10^{-7}$	2632.0609
10		$2.4095 \cdot 10^{-8}$	
11		$1.3194 \cdot 10^{-9}$	

The plate is discretised by hexahedral elements with MSC.Patran2010.2. The number of nodes is equal to 1440 and the number of elements is 600. The applied force is set to 3500 units of force and decomposed in 20 load steps in the direct computation. The isotropic elastoplastic material parameters used in the simulation are summarised in Table 1. The computation of the recursive method took 17 minutes 30 seconds. Five iterations were needed to reach ε . The Δ values introduced in Equation 33 computed after each iteration are summarised in Table 4 and plotted in Figure 10 (blue curve). It can be observed that the rate of convergence is almost linear. The finally obtained undeformed configuration of the plate is illustrated in Figure 11(A) with loads and boundary conditions is plotted. A zoom of the top of plate is plotted in Figure 11(B) to better see the deformation. The direct mechanical computation with this final undeformed configuration as an input is shown in Figure 11(C) with the equivalent plastic strain (-).

Discussion

In this section the influence in the choice of the starting value (initialisation of the recursive formulation) for the set of internal variables on the bar, the Cook's membrane and the circular plate is discussed. We used for a more convenient implementation constant single numerical values for the starting set of internal variables instead of a non homogeneous field.





Influence of the starting values of the internal variables on the bar

The presented method was computed as in the previous section but this time the internal variables were first initialised to $\{E^p, \alpha\} = \{0, 0.4\}$ and subsequently to $\{E^p, \alpha\} = \{0.1, 0\}$. It was found that the computation took 10 minutes 40 seconds when $\{E^p, \alpha\} = \{0, 0.4\}$. The convergence tolerance ε was obtained after nine iterations (Table 2). The values Δ after each iterations are plotted in Figure 4 (black curve).

For this case the computation took three additional iterations and additional 4 minutes 37 seconds to converge, than when the starting set of internal variables was initialised to zero. Furthermore, if the undeformed position of the nodes obtained with both starting values of the internal variables is compared, it was found that

$$\Delta = \|X_{\{E^p, \alpha\}=\{0,0\}} - X_{\{E^p, \alpha\}=\{0,0.4\}}\|^2 = 2.4810^{-10}, \quad (35)$$

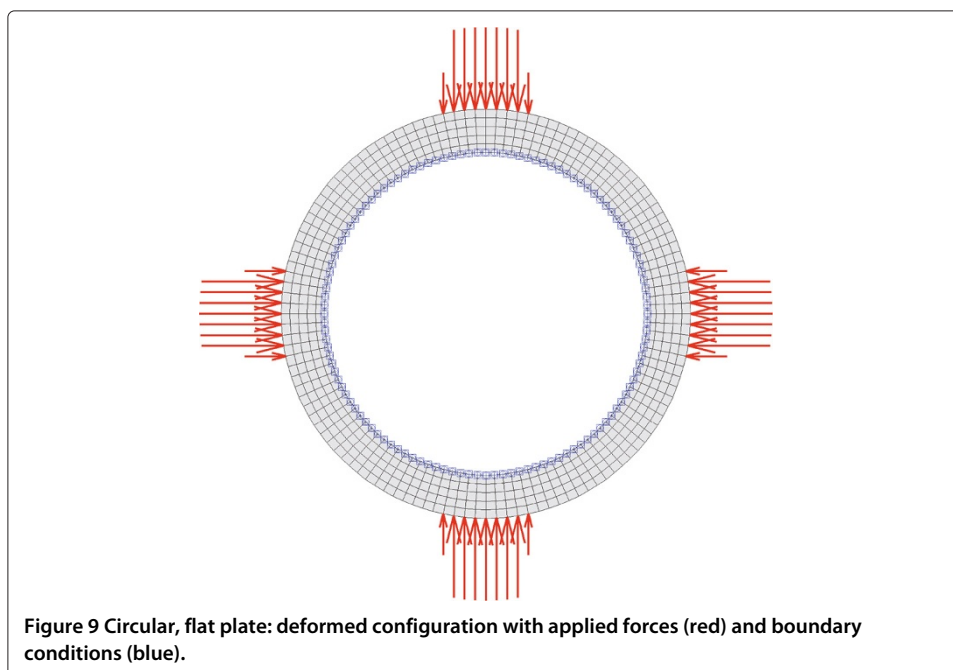


Table 4 Circular plate: Convergence

Circular plate: Calculation of Δ			
Iteration	$\{E^p, \alpha\} = \{0, 0\}$	$\{E^p, \alpha\} = \{0, 0.1\}$	$\{E^p, \alpha\} = \{-0.1, 0\}$
1	$1.897 \cdot 10^{-2}$	13.3091	88.913
2	$2.0153 \cdot 10^{-4}$	$5.9613 \cdot 10^{-3}$	11.4455
3	$2.1253 \cdot 10^{-6}$	$1.8077 \cdot 10^{-4}$	22.8091
4	$4.1797 \cdot 10^{-8}$	$1.3011 \cdot 10^{-6}$	50.1605
5	$4.4199 \cdot 10^{-10}$	$4.3398 \cdot 10^{-8}$	129.4614
6		$9.6423 \cdot 10^{-10}$	

i.e., the difference is negligible. In the case where $\{E^p, \alpha\} = \{0.1, 0\}$ the computation was stopped after nine iterations because of the divergence of the Δ values. The Δ values after each iterations are plotted in Figure 4 (red curve). We conclude that the initial values of the internal variables chosen for the computation of the recursive formulation have an influence on the computational costs and on the number of iterations needed to reach the convergence but not on the final result, i.e., on the sought undeformed configuration of the bar, if convergence can be achieved.

Influence of the starting values of the internal variables on the Cook’s membrane

The presented method was computed as in the previous section but this time the internal variables were first initialised to $\{E^p, \alpha\} = \{0, 0.1\}$ and subsequently to $\{E^p, \alpha\} = \{0.02, 0.02\}$. It was found that the computation took 5 hours 23 minutes 34 seconds for the first case. The convergence tolerance ε was obtained after 11 iterations (Table 3). The values Δ after each iterations are plotted in Figure 7 (red curve). It can be observed that the rate of convergence is almost linear.

For this case the computation took two additional iterations and additional 35 minutes 19 seconds to converge, than when the starting set of internal variables was initialised to zero. Furthermore, if the undeformed position of the nodes obtained with both starting values of the internal variables is compared, it was found that

$$\Delta = \|X_{\{E^p, \alpha\}=\{0,0\}} - X_{\{E^p, \alpha\}=\{0,0.1\}}\|^2 = 1.8610^{-7}, \tag{36}$$

i.e., the difference is negligible. In the case where $\{E^p, \alpha\} = \{0.02, 0.02\}$ the computation was stopped after nine iterations because of the divergence of the Δ values. The Δ values

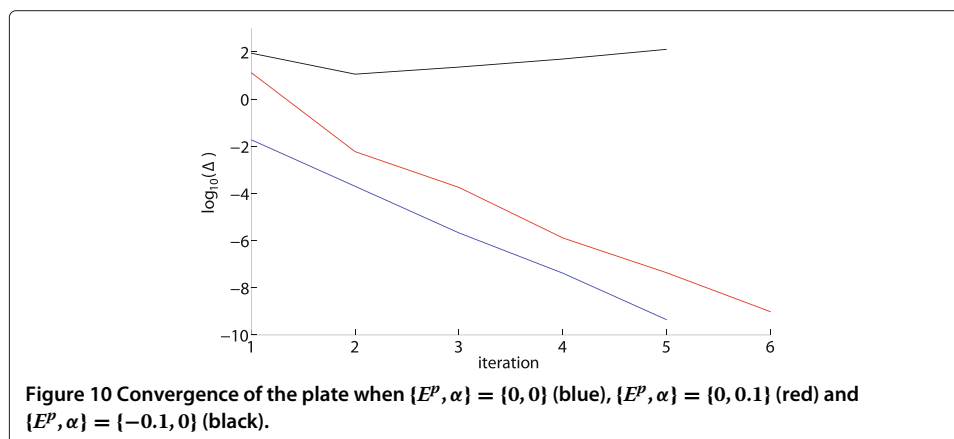
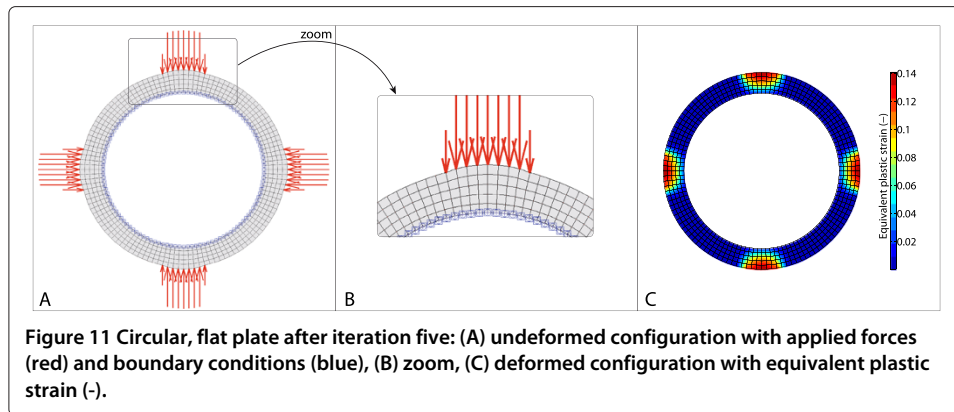


Figure 10 Convergence of the plate when $\{E^p, \alpha\} = \{0, 0\}$ (blue), $\{E^p, \alpha\} = \{0, 0.1\}$ (red) and $\{E^p, \alpha\} = \{-0.1, 0\}$ (black).



after each iterations are plotted in Figure 7 (black curve). We conclude that the initial values of the internal variables chosen for the computation of the recursive formulation have an influence on the computational costs and on the number of iterations needed to reach the convergence but not on the final result, i.e., on the sought undeformed configuration of the Cook's membrane, if convergence can be achieved.

Influence of the starting values of the internal variables on the circular, flat plate

The presented method was computed as in the previous section but this time the internal variables were first initialised to $\{E^p, \alpha\} = \{0, 0.1\}$ and subsequently to $\{E^p, \alpha\} = \{-0.1, 0\}$. It was found that the computation took 21 minutes 57 seconds for the first case. The convergence tolerance ε was obtained after six iterations (Table 4). The values Δ after each iterations are plotted in Figure 10 (red curve). It can be observed that the rate of convergence is almost linear.

For this case the number of iterations is equal to the case, where the set of internal variables was initialised to zero, but the computation took 4 minutes 27 seconds longer. Furthermore, if the undeformed position of the nodes obtained with both starting values of the internal variables is compared, it was found that

$$\Delta = \|\mathbf{X}_{\{E^p, \alpha\}=\{0,0\}} - \mathbf{X}_{\{E^p, \alpha\}=\{0,0.1\}}\|^2 = 3.1510^{-10}, \quad (37)$$

i.e., the difference is negligible. In the case where $\{E^p, \alpha\} = \{-0.1, 0\}$ the computation was stopped after five iterations because of the divergence of the Δ values. The Δ values after each iterations are plotted in Figure 10 (black curve). We conclude that the initial values of the internal variables chosen for the first computation of the recursive formulation have an influence on the computational costs, but not on the final result, i.e., on the sought undeformed configuration of the circular, flat plate, if convergence can be achieved.

Conclusion

In this contribution a new method for solving inverse form finding problems for isotropic elastoplastic materials is presented. To that end, a recursive formulation is deployed to find the desired undeformed configuration of the functional component. The inverse mechanical formulation in elastoplasticity is first performed on the target deformed configuration of the workpiece with the set of internal variables initialised to a homogeneous field equal to zero. Subsequently, a direct mechanical formulation on the computed undeformed configuration is used, which ensures the path-dependency in elastoplasticity. The

obtained deformed configuration is furthermore compared with the target deformed configuration of the component. If the difference is negligible, the wanted undeformed configuration of the functional component is obtained. Otherwise the computation of the elastoplastic inverse mechanical formulation is started again with the target deformed configuration and the current heterogeneous state of internal variables obtained at the end of the computed direct formulation. This process is continued until convergence is reached. Three numerical examples, a bar, the Cook's membrane and a circular, flat plate in 3D illustrated this recursive formulation for finding the corresponding undeformed configurations in isotropic elastoplasticity. The convergence was reached after six, nine and five iterations, respectively, when initialising the set of internal variables to zero at the beginning of the computation. The influence of the starting values for the set of internal variables at the beginning of the computation was afterwards discussed. It was found that when the initial set of internal variables was initialised to zero at the beginning of the computation the convergence was reached after less iterations and less computational time than with other values. The rates of convergence were almost linear. The computation of the three numerical examples with the recursive formulation did not converge for one value of the set of internal variables and had to be stopped. Comparing the results of the numerical examples, it was demonstrated that different starting values for the set of internal variables have no influence on the obtained undeformed configuration. We conclude that the choice of the initial set of internal variables has an influence on the convergence evolution but not on the result, if convergence can be achieved. Therefore an initial homogeneous set of internal variables equal to zero, which is a natural choice in programming since the set of internal variables is unknown at the beginning of the computation, should be considered for such problems. An extension of the presented new method for solving inverse form finding problems to anisotropic elastoplasticity will be of great interest for metal forming processes.

Competing interests

The authors declare that they have no competing interests.

Authors' contributions

SG: conception and design of the study, analysis and interpretation of data, drafted the manuscript. PL: revised of the manuscript. PS: study supervision, revision of the manuscript. All authors read and approved the final manuscript.

Acknowledgements

This work is supported by the German Research Foundation (DFG) under the Transregional Collaborative Research Center SFB/TR73: "Manufacturing of Complex Functional Components with Variants by Using a New Sheet Metal Forming Process - Sheet-Bulk Metal Forming".

Received: 22 August 2013 Accepted: 4 April 2014

Published: 11 April 2014

References

1. Govindjee S, Mihalic P (1996) Computational methods for inverse finite elastostatics. *Comput Methods Appl Mech Eng* 136(1-2): 47-57
2. Govindjee S, Mihalic P (1998) Computational methods for inverse deformations in quasi-incompressible finite elasticity. *Int J Numerical Methods Eng* 43(5): 821-838
3. RT Shield R (1967) Inverse deformation results in finite elasticity. *Zeitschrift für angewandte Mathematik und Physik* 18: 490-500
4. Govindjee S (1999) Finite deformation inverse design modeling with temperature changes, axis-symmetry and anisotropy. In Report Number UCB/SEMM-1999/01, University of California, Berkeley
5. Koishi M, Govindjee S (2001) Inverse design methodology of a tire. *Tire Sci Technol* 29(3): 155-170
6. Yamada T (1998) Finite element procedure of initial shape deformation for hyperelasticity. *Struct Eng Mech* 6: 173-183
7. Fachinotti V, Cardona A, Jetteur P (2008) Finite element modelling of inverse design problems in large deformations anisotropic hyperelasticity. *Int J Numerical Methods Eng* 74(6): 894-910

8. Fachinotti V, Cardona A, Jetteur P (2006) A finite element model for inverse design problems in large deformations anisotropic hyperelasticity. In: Cardona A, Nigro N, Sonzogni V, Storti M (eds) *Mecánica Computacional*, November 2006, Santa Fe, pp 1269–1284
9. Albanesi A, Fachinotti V, Cardona A (2010) Inverse finite element method for large-displacement beams. *Int J Numerical Methods Eng* 84: 1166–1182
10. Albanesi A, Fachinotti V, Pucheta M (2010) A review on design methods for compliant mechanisms. In: Dvorkin E, Goldschmit M, Storti M (eds) *Mecánica Computacional*, 15–18 November 2010, Buenos Aires, pp 59–72
11. Lu J, Zhou X, Raghavan M (2007) Computational method of inverse elastostatics for anisotropic hyperelastic solids. *Int J Numerical Methods Eng* 69: 1239–1261
12. Zhou X, Lu J (2008) Inverse formulation for geometrically exact stress resultant shells. *Int J Numerical Methods Eng* 74: 1278–1302
13. S, Scherer M, Steinmann P (2010) On inverse form finding for anisotropic hyperelasticity in logarithmic strain space. *Int J Struct Changes Solids - Mech Appl* 2(2): 1–16
14. Germain S, Scherer M, Steinmann P (2010) On inverse form finding for anisotropic materials. In: Wieners C (ed) *Proceedings in Applied Mathematics and Mechanics: 81st Annual Meeting of the International Association of Applied Mathematics and Mechanics (GAMM)*, 22–26 March 2010, Karlsruhe, pp 159–160
15. Germain S (2013) On inverse form finding for anisotropic materials in the logarithmic strain space. PhD thesis, Chair of Applied Mechanics, University of Erlangen-Nuremberg
16. Germain S, Steinmann P (2011) On inverse form finding for anisotropic elastoplastic materials. *AIP Conf Proc* 1353: 1169–1174
17. Germain S, Steinmann P (2011) Shape optimization for anisotropic elastoplasticity in logarithmic strain space. In: Oñate E, Owen D, Peric D, Suárez B (eds) *Computational Plasticity XI - Fundamentals and Applications*: 7-11 September 2011, Barcelona, pp 1479–1490
18. Germain S, Steinmann P (2012) Towards inverse form finding methods for a deep drawing steel DC04. *Key Eng Mater* 504–506: 619–624
19. Germain S, Steinmann P (2012) On a recursive algorithm for avoiding mesh distortion in inverse form finding. *J Serbian Soc Comput Mech* 6: 216–234
20. Germain S, Steinmann P (2011) A comparison between inverse form finding and shape optimization methods for anisotropic hyperelasticity in logarithmic strain space. In: Brenn G, Holzapfel GA, Schanz M, Steinbach O (eds) *Proceedings in Applied Mathematics and Mechanics: 82nd Annual Meeting of the International Association of Applied Mathematics and Mechanics (GAMM)*, 18-21 April 2011, Graz, pp 367–368
21. Germain S, Steinmann P (2012) On two different inverse form finding methods for hyperelastic and elastoplastic materials. In: Alber HD, Kraynyukova N, Tropea C (eds) *Proceedings in Applied Mathematics and Mechanics: 83rd Annual Meeting of the International Association of Applied Mathematics and Mechanics (GAMM)*, 26-30 March 2012, Darmstadt, pp 263–264
22. Ibrahimbegovic A, Knopf-Lenoir C, Kucerova A, Villon P (2004) Optimal design and optimal control of elastic structures undergoing finite rotations. *Int J Numerical Methods Eng* 61(14): 2428–2460
23. Ibrahimbegovic A, Knopf-Lenoir C (2003) Shape optimization of elastic structural systems undergoing large rotations: simultaneous solution procedure. *Comput Model Eng Sci* 4: 337–344
24. Sousa LC, Castro CF, António CAC, Santos AD (2002) Inverse methods in design of industrial forging processes. *Journal* 128: 266–273
25. Ponthot JP, Kleinermann JP (2006) A cascade optimization methodology for automatic parameter identification and shape/process optimization in metal forming simulation. *Comput Methods Appl Mech Eng* 195: 5472–5508
26. Ask A, Denzer R, Menzel A, Ristinmaa M (2013) Inverse-motion-based form finding for quasi-incompressible finite electroelasticity. *Int J Numerical Methods Eng* 94(6): 554–572
27. Green AE, Naghdi PM (1965) A general theory of an elastic-plastic continuum. *Arch Ration Mech Anal* 18: 251–281
28. Lee EH (1969) Elastic-plastic deformation at finite strains. *J Appl Mech* 36: 1–14
29. Naghdi PM (1990) A critical review of the state of finite plasticity. *J Appl Math Phys* 41: 315–394
30. Casey J, Naghdi PM (1980) A remark on the use of the decomposition $F=FeFp$ in plasticity. *J Appl Mech* 47: 672–675
31. Ibrahimbegovic A (2009) *Nonlinear solid mechanics: Theoretical formulations and finite element solution methods*. Springer, Dordrecht Heidelberg London New York
32. de Souza Neto EA, Perić D, Owen DRJ (2008) *Computational Methods for Plasticity - Theory and Applications*. John Wiley & Sons Ltd, Chichester, UK
33. Simo JC, Hughes TJR (1998) *Computational Inelasticity*. Springer-Verlag New York, Inc., New York
34. Lubliner J (2008) *Plasticity Theory*. Dover Publications, Inc., Mineola, NY, USA
35. Miehe C, Apel N, Lambrecht M (2002) Anisotropic additive plasticity in the logarithmic strain space: modular kinematic formulation and implementation based on incremental minimization principles for standard materials. *Comput Methods Appl Mech Eng* 191(47–48): 5383–5425
36. Apel N (2004) Approaches to the description of anisotropic material behaviour at finite elastic and plastic deformations, theory and numerics. PhD thesis, Stuttgart University, Institute of Applied Mechanics (Chair I)
37. Miehe C, Apel N (2004) Anisotropic elastic-plastic analysis of shells at large strains. A comparison of multiplicative and additive approaches to enhances finite element design and constitutive modelling. *Int J Numerical Methods Eng* 61: 2067–2113
38. Miehe C, Lambrecht M (2001) Algorithms for computation of stresses and elasticity moduli in terms of Seth–Hill’s family of generalized strain tensors. *Commun Numerical Methods Eng* 17: 337–353

doi:10.1186/2213-7467-1-10

Cite this article as: Germain et al.: On a recursive formulation for solving inverse form finding problems in isotropic elastoplasticity. *Advanced Modeling and Simulation in Engineering Sciences* 2014 **1**:10.